Acta Biochim Biophys Sin xxxx, xx(x): xx-xx
https://cstr.cn/32197.14.abbs.2026092
https://doi.org/10.3724/abbs.2026092
Original Article

Original Article

MAERL accelerates atherosclerosis by inhibiting macrophage efferocytosis via transglutaminase 2

Kun Xiao[1,2,3,†], Yajing Wang[1,†], Qianqian Wu[1,4,†], Zhenghao Zhang[5], Shujuan Li[6], Jiaqi Yang[1], Xiangyu Zhao[1], Guizhong Li[1,2], Jianmin Sun[1,4], Fang Ma[1,2,6,*], Shengchao Ma[1,2,*], and Guodong Zhang[7,*]

[1]NHC Key Laboratory of Metabolic Cardiovascular Diseases Research, Ningxia Medical University, Yinchuan 750004, China, [2]Ningxia Key Laboratory of Vascular Injury and Repair Research, Ningxia Medical University, Yinchuan 750004, China, [3]Luoyang Central Blood Bank, Luoyang 471000, China, [4]School of Basic Medical Sciences, Ningxia Medical University, Yinchuan 750004, China, [5]Department of Otolaryngology Head and Neck Surgery, Ningxia People's Hospital of Ningxia Hui Autonomous Regin, Yinchuan 750002, China, [6]Clinical Medical School, Ningxia Medical University, Yinchuan 750004, China, and [7]Science and Technology Center, Ningxia Medical University, Yinchuan 750004, China

[†]These authors contributed equally to this work.

*Correspondence address. E-mail: 25011012@nxmu.edu.cn (F.M.); solarmsc@163.com (S.M.); 20130112@nxmu.edu.cn (G.Z.)

Received 24 December 2025 Accepted 11 May 2026 Published 14 October 2026

Abstract

Atherosclerotic cardiovascular and cerebrovascular diseases continue to represent the leading cause of global disease burden and mortality. Defective efferocytosis the phagocytic clearance of apoptotic cells by macrophages, is a well-established pathological mechanism that fuels chronic inflammation and drives necrotic core expansion in atherosclerotic plaques. Hyperhomocysteinemia (HHcy) is an independent risk factor for atherosclerosis development. However, the role of long non-coding RNAs (lncRNAs) induced by homocysteine (Hcy) in this process remains largely unexplored. Here, we demonstrate that Hcy impairs macrophage efferocytosis and enhances inflammation in atherosclerosis, both in high methionine diet (HMD)-fed *ApoE*$^{-/-}$ mice and in RAW264.7 cells treated with Hcy. We further identify a markedly up-regulated lncRNA in Hcy-induced macrophages, termed macrophage efferocytosis-related lncRNA (MAERL). Knockdown of *MAERL* attenuates the impairment of efferocytosis and reduces inflammation. Mechanistically, MAERL interacts with and inhibits transglutaminase 2 (TGM2), thereby significantly suppressing macrophage efferocytosis and promoting inflammation. Collectively, these findings reveal a MAERL/TGM2 pathway in macrophages as a key regulatory mechanism in the development of atherosclerosis.

Key words lncRNA MAERL, transglutaminase 2 (TGM2), homocysteine, macrophage efferocytosis, atherosclerosis

Introduction

Hyperhomocysteinemia (HHcy) is an independent risk factor for the development of atherosclerosis, contributing to various cardiovascular and cerebrovascular diseases, such as coronary heart disease, stroke, peripheral artery disease, thrombosis, and myocardial infarction [1,2]. Atherosclerosis-related diseases account for 20% of global mortality [3]. However, the precise molecular mechanisms through which Hcy promotes atherosclerosis remain incompletely understood. Discovering novel regulatory targets for Hcy-induced atherosclerosis is crucial for the future development of strategies to prevent and treat atherosclerotic cardiovascular diseases. During the progression of atherosclerosis, macrophage efferocytosis is a critical mechanism for clearing apoptotic cells (ACs) and maintaining plaque stability. Proteins such as those in the T cell immunoglobulin and mucin domain (TIM) family, low-density lipoprotein-related protein-1(LRP1), MER proto-oncogene tyrosine kinase (MerTK), milk fat globule-EGF factor 8 (MFG-E8) and transglutaminase 2 (TGM2), have been shown to play crucial roles in macrophage efferocytosis, mediating the clearance of ACs [4]. Efficient efferocytosis promptly removes ACs within the plaque, thereby inhibiting necrotic core formation and promoting inflammatory resolution [5]. Accordingly, failed or ineffective efferocy-

© The Author(s) 2026. This is an open access article distributed under the terms of the Creative Commons Attribution-NonCommercial-NoDerivs License (https://creativecommons.org/licenses/by-nc-nd/4.0/).

tosis leads to secondary necrosis of ACs, resulting in the release of damage-associated molecular patterns that exacerbate intraplaque inflammation and drive the expansion of the necrotic core [4].

Long non-coding RNAs (lncRNAs) are transcripts longer than 200 nucleotides with limited or no protein-coding capacity. Despite their lack of protein-coding potential, lncRNAs have emerged as key regulators across diverse biological systems, influencing processes such as development, metabolism, and disease pathogenesis. Their mechanisms of action are remarkably versatile, ranging from chromatin modification and genomic imprinting to transcriptional and post-transcriptional regulation, acting both in *cis* and *trans* and modulating the subcellular localization of transcription factors [6,7]. Increasing evidence has demonstrated that lncRNAs exert pivotal regulatory effects on the development and progression of atherosclerosis [8]. For example, MIR181A1HG induces vascular inflammation in atherosclerosis by decoying Foxp1 away from target gene promoters and activating the NLRP3 inflammasome [9]; lncRNA RP4-639F20.1 interacts with THRAP3 to attenuate atherosclerosis, and lncRNA Gpr137b-ps promotes advanced atherosclerosis via the regulation of autophagy [10]. Interestingly, the expression of a specific subset of lncRNAs can be influenced by pathological microenvironmental factors such as Hcy. Our previous study elucidated the protective mechanisms of lncARF against the development of atherosclerosis, which physically binds to RRAGD and further activates the PI3K/Akt and MAPK signaling pathways [11]. However, the mechanisms of its regulatory function in cardiovascular pathogenesis remain unknown. Therefore, further studies are warranted to identify and characterize functional lncRNAs that are implicated in the progression of atherosclerosis.

In this study, we identified that homocysteine (Hcy) inhibits macrophage efferocytosis and promotes inflammation in atherosclerosis, both in high methionine diet (HMD)-fed *ApoE*$^{-/-}$ mice and in RAW264.7 cells treated with Hcy. lncRNA microarray profiling was performed to identify differentially expressed lncRNAs induced by Hcy. A specific lncRNA, MSTRG.2814.24, which we named macrophage efferocytosis-related lncRNA (MAERL), was found to be markedly upregulated in Hcy-treated macrophages. Functional investigations revealed that MAERL significantly impairs macrophage efferocytosis and enhances inflammation by interacting with and inhibiting TGM2. Our findings uncover a previously uncharacterized lncRNA that exerts an anti-efferocytosis function in macrophages during atherosclerosis, providing important new insights into the functional roles and therapeutic potential of lncRNAs in atherosclerosis.

Materials and Methods

Animals

Six-week-old male apolipoprotein E knockout (*ApoE*$^{-/-}$) C57BL/6J mice were sourced from Charles River (Beijing, China). Following a two-week acclimatization period, the mice were randomly assigned to two dietary regimens: (1) normal diet (ND) containing 20% protein, 4.5% fat, and 55.5% carbohydrate; and (2) HMD, consisting of the ND supplemented with 1.7% methionine. The animals were housed under controlled conditions (22–25°C, 45% humidity; 12-h light-dark cycle) in groups of six per cage. After 16 weeks of dietary intervention, the mice were anesthetized, and tissues were harvested for subsequent analysis. All procedures were approved by the Animal Care and Use Committee of Ningxia Medical University (ethics approval number: 2025-G078) and conducted in accordance with institutional guidelines.

Cell culture and transfection

RAW264.7 cells were obtained from the Cell Resource Center of the Shanghai Institute for Biological Sciences (Shanghai, China). Cells were maintained in Dulbecco's modified Eagle's medium (DMEM; HyClone, Logan, USA) supplemented with 10% fetal bovine serum (FBS; Gibco, Carlsbad, USA) and 1% penicillin/streptomycin (Solarbio, Beijing, China) and incubated at 37°C in a humidified atmosphere containing 5% CO_2. For transfection studies, small interfering RNAs (siRNAs) targeting transglutaminase 2 (TGM2; siTGM2: 5′-CAGAGTCAAACCTCATCAA-3′) and negative control (si-NC: 5′-TTCTCCGAACGTGTCACGT-3′) were sourced from GenePharma (Shanghai, China), and MAERL-specific LNA GapmeRs (LNA-MAERL 1: 5′-CGTCCTTCCTCCTCGC-3′; LNA-MAERL 2: 5′-GCGTCCTTCCTCCTCG-3′; and LNA-NC: 5′-GCTCCCTTCAATC CAA-3′) were acquired from Qiagen (Hilden, Germany). Transient transfections were performed using Lipofectamine 2000 reagent (Invitrogen, Carlsbad, USA) following the manufacturer's protocol.

Immunofluorescence staining

Frozen sections of aortic roots at the valve level were allowed to equilibrate to room temperature and examined for tissue integrity. Sections were fixed in 4% paraformaldehyde for 30 min, followed by three washes with PBS. Endogenous peroxidase activity was blocked by incubating sections in 10% hydrogen peroxide for 8 min. For permeabilization, sections were treated with 0.3% Triton X-100 for 10 min at room temperature. Non-specific binding was blocked with goat serum for 60 min at room temperature. Sections were then incubated overnight at 4°C with primary antibodies anti-F4/80 (1:500, AG4753; Beyotime, Shanghai, China), anti-MerTK (1:50, Ab300136; Abcam, Cambridge, UK), and anti-Caspase-3 (1:200, 9662S; Cell Signaling Technology, Danvers, USA). After three PBS washes, sections were incubated with FITC-conjugated (1:1000, 740178MP555; Santa Cruz, Santa Cruz, USA) and Cy3-conjugated secondary antibodies (1:1000, MA569638; Santa Cruz) for 60 min at room temperature. Following three additional PBS washes, nuclei were counterstained with DAPI for 15 min in the dark. Sections were washed three times with PBS, mounted with an anti-fade mounting medium, and coverslipped. Fluorescence images were captured using an FV1200MPE fluorescence microscope (Olympus, Tokyo, Japan). Immunofluorescence intensity of the aortic root plaque was quantified using ImageJ software.

TUNEL assay

Frozen sections of aortic roots were allowed to equilibrate to room temperature and examined for tissue integrity. TUNEL staining was performed according to the manufacturer's instructions. Briefly, sections were co-stained with anti-F4/80 antibody, TUNEL reaction mixture (Roche, Basel, Switzerland) and DAPI. After staining, sections were mounted with an anti-fade mounting medium and coverslipped. Fluorescence images were acquired using the FV1200MPE fluorescence microscope. The TUNEL fluorescence intensity and colocalization with F4/80-positive macrophages within plaques were analyzed using ImageJ software.

lncRNA sequencing

Total RNA was isolated from macrophages with TRIzol reagent (TIANGEN, Beijing, China). lncRNA sequencing was conducted by

Beijing Biomarker Technologies Corporation (Beijing, China) following the manufacturer's standard procedures. Raw data and array images were processed using Agilent Feature Extraction software (version 11; Agilent, Santa Clara, USA). Subsequent RNA quantification and data analysis were performed with GeneSpring GX v12.0 (G2565BA; Agilent). Differentially expressed lncRNAs were identified based on a fold change ≥ 1.5 and a P value < 0.05.

Bioinformatic analysis

The protein-binding partners of the lncRNA MAERL were predicted using the catRAPID omics v2.0 module (http://service.tartaglialab.com/page/catrapid_group). The human FASTA sequence of the lncRNA was obtained from the lncRNA-seq. Analysis was performed against the human reference proteome with default parameters. Predicted interactors were ranked by an integrated star-rating system based on normalized interaction propensity, the presence of RNA/DNA-binding domains and disordered regions, and known RNA-binding motifs.

Coding potential of MAERL was predicted using Coding Potential Assessment Tool (CPAT) (http://lilab.research.bcm.edu/cpat/) and Coding Potential Calculator 2 (CPC2) (http://cpc2.gao-lab.org/) algorithms with ACTA1, GAPDH as protein-coding controls and HOTAIR, TUG1 as lncRNA controls, while its chromosomal localization and cross-species conservation among higher mammals were annotated via the UCSC Genome Browser (https://genome.ucsc.edu/).

Fluorescence *in situ* hybridization (FISH) and immunofluorescence

A FISH assay was performed using LncRNA FISH Probe Mix (RiboBio, Guangzhou, China). Briefly, macrophages were fixed with 4% paraformaldehyde (Solarbio) and sequentially treated with proteinase K, glycine, and acetylation reagents. Following a 30-min prehybridization at 37°C, the cells were hybridized overnight at 37°C with Cy3-labeled MAERL probes. Nuclei were counterstained with DAPI. Images were captured using an LSM900 confocal laser-scanning microscope (Zeiss, Oberkochen, Germany).

RNA isolation from the nuclear and cytoplasmic fractions

The nuclear and cytoplasmic RNA of macrophages was isolated using the Ambion® PARIS™ Kit (Thermo Scientific, Waltham, USA). Briefly, cultured cells were homogenized in ice-cold cell disruption buffer to obtain a total cell lysate. Rapid homogenization on ice in the presence of detergent allowed simultaneous recovery of protein and RNA directly from the lysate. For RNA extraction, an equal volume of lysis/binding solution was immediately added to a portion of the lysate. Total RNA was then purified through an RNA-binding glass fiber filter, followed by three rapid wash steps, and finally eluted in a concentrated form. Subsequently, RNA from the nuclear and cytoplasmic fractions was subjected to qRT-PCR analysis.

qRT-PCR

Total RNA was isolated from macrophages using TRIzol reagent (TIANGEN) following the manufacturer's standard protocol. The purified RNA was reverse transcribed into cDNA using PrimeScript RT Master Mix (TaKaRa, Dalian, China). Quantitative PCR was carried out with TB Green qPCR Master Mix (TaKaRa) on a Real-Time PCR detection system (Thermo Scientific) in a total reaction volume of 20 μL. The amplification protocol consisted of an initial denaturation at 95°C for 30 s, followed by 35 cycles of 95°C for 5 s and annealing/extension at 72°C for 34 s. Relative gene expression was determined using the $2^{-\Delta\Delta Ct}$ method with normalization to the housekeeping gene *GAPDH*. The primer sequences are presented in Table 1.

Rapid amplification of cDNA ends (RACE)

The full-length cDNA of MAERL was amplified from macrophage RNA using the SMARTer RACE 5′/3′ kit (TaKaRa). Nested 5′ and 3′ RACE products were generated with the GeneRacer™ kit (Invitrogen). Amplified fragments were purified with the SanPrep Column DNA Gel Extraction Kit (Sangon Biotech, Shanghai, China), cloned and inserted into the pGM-T vector, and verified by Sanger sequencing.

Western blot analysis

Total protein was extracted by lysing cells in a buffer supplemented with protease inhibitor, phosphatase inhibitor, and PMSF (Keygen Biotech, Nanjing, China). Equal amounts of protein (30 μg) were

Table1. The sequences of the primers used in this study

lncRNA or gene	Strand	Primer sequence
ENST00000502041	Forward	5′-GAGATAGACGGGAAGATCGGTAGGG-3′
	Reverse	5′-GGACTTGCCTCTGCCTGGAATG-3′
ENST00000418833	Forward	5′-GCGTCGTGTCTTCAGTCCTTATCG-3′
	Reverse	5′-CAGTCATCCCTCCACCCGTCTC-3′
MSTRG.12698.1	Forward	5′-TAGCCCATGACTACACAAGTGCAAC-3′
	Reverse	5′-CCCGCATCTCTTCCTTTCACATCC-3′
MSTRG.86666.2	Forward	5′-CGGTCCTAGCCTGCCTGTACG-3′
	Reverse	5′-CTGGAGCCTGGGAGGTGGAAG-3′
MSTRG.2814.24	Forward	5′-TTTCTCTTGCCACTGCCGTGTAAG-3′
	Reverse	5′-TGGGAGGCTGTGACATTGACAAAG-3′
MSTRG.39103.21	Forward	5′-GACCAGCCTCGGCAACATAGTG-3′
	Reverse	5′-AATCCTCCCACCTCAGCCTTCAG-3′
MSTRG.88917.16	Forward	5′-AGGAGGCGGGAACCGAAGAAG-3′
	Reverse	5′-CGTCCTTCCTCCTCGCTCCTC-3′
Tnf-α	Forward	5′-CAGGCGGTGCCTATGTCTC-3′
	Reverse	5′-CGATCACCCCGAAGTTCAGTAG-3′
Il-6	Forward	5′-CTGCAAGAGACTTCCATCCAG-3′
	Reverse	5′-AGTGGTATAGACAGGTCTGTTGG-3′
Ccl2	Forward	5′-TAAAAACCTGGATCGGAACCAAA-3′
	Reverse	5′-GCATTAGCTTCAGATTTACGGGT-3′
Arg1	Forward	5′-CTCCAAGCCAAAGTCCTTAGAG-3′
	Reverse	5′-GGAGCTGTCATTAGGGACATCA-3′
Il-10	Forward	5′-CTTACTGACTGGCATGAGGATCA-3′
	Reverse	5′-GCAGCTCTAGGAGCATGTGG-3′
TGM2	Forward	5′-GCTGGACCAACAGGACAATGT-3′
	Reverse	5′-CTCTAGGCTGAGACGGTACAG-3′
GAPDH	Forward	5′-GGAGCGAGATCCCTCCAAAAT-3′
	Reverse	5′-GGCTGTTGTCATACTTCTCATGG-3′

separated by 10% SDS-PAGE and transferred onto PVDF membranes (Millipore, Billerica, USA). After blocking with 5% BSA in PBST for 4 h at 4°C and washing three times with DPBS, the membranes were incubated overnight at 4°C with the indicated primary antibodies. The primary antibodies used were as follows: TGM2 (1:1000, Ab2386; Abcam), EEF1A2 (1:1000, 66806-1-Ig; Proteintech, Wuhan, China) and β-actin (1:10000, sc-47778; Santa Cruz). Following another wash step, the membranes were probed with the corresponding HRP-conjugated secondary antibodies: HRP goat anti-rabbit IgG (H+L) (1:5000, AB0101; Abways, Shanghai, China) or HRP goat anti-mouse IgG (H+L) (1:5000, AB0102; Abways). Protein bands were visualized using the ChemiDoc™ XRS+ System (1708265; Bio-Rad, Hercules, USA).

RNA pull-down assay

Biotin-labeled MAERL RNA was synthesized *in vitro* by RiboBio. Briefly, the biotinylated RNA was incubated with fibroblast lysate (2 mg total protein) in RIP buffer (Thermo Scientific) under gentle rotation at room temperature for 1 h. Subsequently, streptavidin magnetic beads (Thermo Scientific) were added, and the mixture was incubated for an additional hour at room temperature. Following rigorous washing with RIP buffer using a magnetic stand, the protein bound to MAERL RNA was eluted and subjected to polyacrylamide gel electrophoresis (PAGE) followed by membrane transfer and immunoblotting (western blot analysis). For mass spectrometric identification, parallel SDS-PAGE gels loaded with identical eluted protein samples were stained using commercial silver staining kit reagents; distinct silver-stained protein bands were manually excised from the gel, fully destained, subjected to in-gel trypsin digestion for enzymatic cleavage of polypeptides, desalted and vacuum-dried. The digested peptide mixtures were reconstituted in mobile phase buffer, separated by reversed-phase liquid chromatography, and then online analyzed by high-resolution mass spectrometry with data-dependent acquisition mode, followed by database searching and bioinformatic annotation of peptide and protein profiles (LC-MS) (Thermo Scientific).

RNA immunoprecipitation (RIP) assay

RIP assay was performed using the RIP RNA-Binding Protein Immunoprecipitation Kit (Millipore). Protein A/G magnetic beads were pre-incubated with 3 μL (≈ 5 μg) of anti-TGM2 antibody or an equal amount of matched IgG isotype control (same host species) at 4°C for 2 h. Cell lysates were then added and incubated with the antibody-bead complexes at 4°C for 3 h with rotation. After washing with 5× wash buffer, immunoprecipitated RNAs were recovered, reverse-transcribed, and analyzed by qRT-PCR to assess TGM2-associated RNA enrichment. Data were normalized to input and expressed as fold enrichment relative to the IgG control (per primer).

Induction of apoptosis in Jurkat cells

Jurkat cells were obtained from the ATCC (Manassas, USA) and cultured in RPMI-1640 medium. Apoptosis was induced by exposing the cells to 254 nm ultraviolet light for 15 min, followed by incubation for 3 h, resulting in an apoptotic rate exceeding 85%. Apoptotic Jurkat cells were then fluorescently labeled by incubation with 2 μM calcein-AM (MKbio, Shanghai, China) for 30 min. Subsequently, macrophages and labeled apoptotic cells were cocultured at a 1:1 ratio for 45 min. After coincubation, nonengulfed apoptotic cells were removed by washing with PBS, and the cells were fixed with 4% paraformaldehyde for 20 min. Fluorescence microscopy was used to capture overlay images of calcein-AM-labeled apoptotic Jurkat cells and macrophages. The phagocytic index was calculated based on the ratio of calcein-AM-positive to calcein-AM-negative effector cells to quantify macrophage efferocytosis.

Immunofluorescence analysis of macrophage efferocytosis

Macrophages from different experimental groups were seeded onto glass-bottom confocal dishes at 60% confluency. Apoptotic Jurkat cells were labeled with PKH26 fluorescent dye (Sigma, St Louis, USA) according to the manufacturer's instructions. Briefly, apoptotic Jurkat cells were resuspended in 1 of mL diluent containing 4 μL of PKH26 fluorescent dye for 5 min. After staining, cells were washed three times with PBS to remove unbound dye, and then cocultured with macrophages at a 1:1 ratio for 45 min at 37°C. After removal of nonengulfed apoptotic cells by washing with PBS, the samples were fixed with paraformaldehyde at 37°C in the dark for 30 min, followed by three times of PBS wash. After blocking with 10% goat serum for 30 min at room temperature, the samples were incubated overnight at 4°C with anti-F4/80 antibody followed by 30 min equilibration at room temperature and PBS washing, incubation with FITC-conjugated secondary antibody (Proteintech), and nuclear staining with DAPI. Coverslips were mounted, and images were captured using the LSM900 confocal laser-scanning microscope.

Statistical analysis

Data analysis was conducted using GraphPad Prism 8. Comparisons between two groups were performed using a two-tailed Student's *t*-test. For comparisons involving multiple treatments across different groups, two-way ANOVA followed by Tukey's multiple comparisons test was employed. For efferocytosis assay, at least 10 random fields were captured from three independent biological replicates in each group. The percentage of efferocytosing macrophages was calculated as the proportion of macrophages containing intracellular PKH26-positive signals among total macrophages. The results are expressed as the mean ± SEM of six independent experiments, and statistical significance was defined as $P < 0.05$.

Results

Hcy inhibits macrophage efferocytosis in atherosclerosis in *ApoE*$^{-/-}$ mice

Macrophage efferocytosis has been recognized as an important step in removing apoptotic cells (ACs), which facilitate the progression of atherosclerosis [12]. *ApoE*$^{-/-}$ mice fed an HMD were used to examine the role of Hcy in efferocytosis in progressing atherosclerosis. It has been reported that caspase 3 activation mediates apoptosis and recruits macrophages, leading to efferocytosis. Thus, the expression of caspase 3 and F4/80 (macrophage markers) was characterized by double immunofluorescence staining in HMD-fed *ApoE*$^{-/-}$ mice. As shown in Figure 1A, a significant increase in caspase 3 was observed in HMD-fed *ApoE*$^{-/-}$ mice, while there was a decrease in colocalization with F4/80 in atherosclerotic plaques. In addition, a lower ratio of TUNEL-positive macrophage-associated cells was also detected in HMD-fed *ApoE*$^{-/-}$ mice, with an increase in TUNEL-positive cells (Figure 1B). This finding was further assessed by the expression of macrophage c-Mer tyrosine kinase

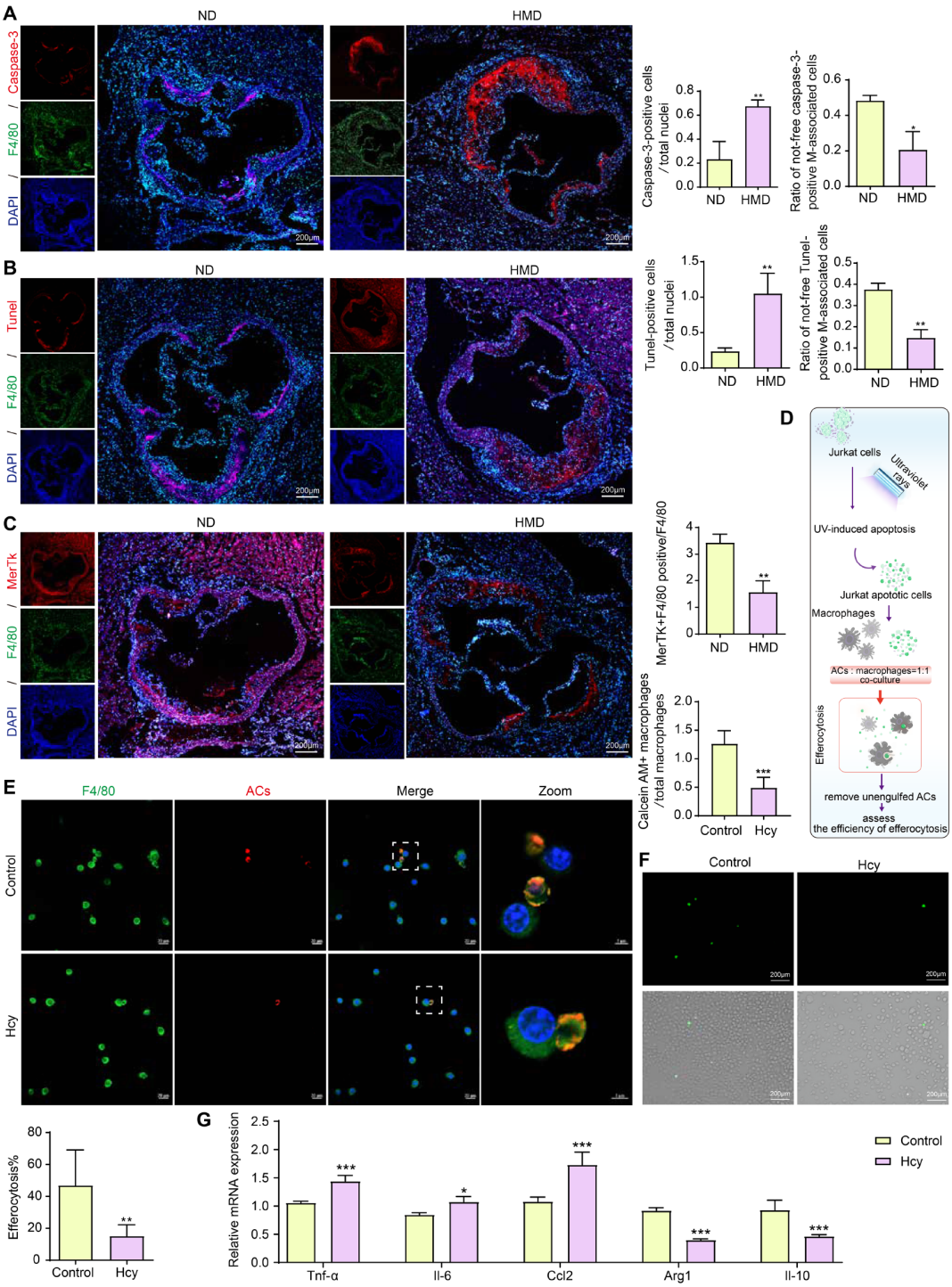

Figure 1. Hcy mediates efferocytosis in atherosclerosis of *ApoE*$^{-/-}$ mice (A) Representative photographs of F4/80 co-localization with caspase-3 in the aorta of *ApoE*$^{-/-}$ mice. Caspase-3 (red), macrophages by F4/80 (green) and nuclei by DAPI (blue). Efferocytosis was assessed as the ratio of free to macrophage-associated caspase-3 positive cells. Scale bar = 200 μm. (B) Representative images of in the aorta of *ApoE*$^{-/-}$ mice in which apoptotic cells were stained by TUNEL (red), macrophages by F4/80 (green) and nuclei by DAPI (blue). Efferocytosis was assessed as the ratio of free to macrophage-associated TUNEL positive cells. Scale bar = 200 μm. (C) Representative fluorescence images of F4/80 (green), MerTK (red) or DAPI (blue) and quantification of the ratio of MerTK/F4/80 co-positive to F4/80 positive macrophages. Scale bar = 200 μm. (D) Flow charts showing the phagocytosis assay protocol used in the *in vitro* studies. Macrophages (Raw 264.7 cells) were tested for phagocytosis of apoptotic Jurkat cells (ACs) after ultraviolet (UV) treatment. (E) Macrophages that had or had not engulfed an ACs were visualized by microscopy, with macrophages (green) were incubated with CFSE-labeled apoptotic cells (red). Scale bar = 20 μm. Zoom, scale bar = 5 μm. (F) *In vitro* efferocytosis assay. Efferocytosis was quantified as the ratio of calcein-positive to calcein-negative macrophages. Scale bar = 200 μm. (G) qRT-PCR was performed to detect the mRNA levels of pro-inflammatory (Il-6, Tnf-α, and Ccl2) and anti-inflammatory genes (Il-10 and Arg1) in macrophages. *$P < 0.05$, **$P < 0.01$, ***$P < 0.001$.

(MerTK), which serves as a cell surface receptor and signaling molecule mediating efferocytosis. The results showed that MerTK expression in lesional macrophages was markedly decreased in HMD-fed *ApoE*$^{-/-}$ mice (Figure 1C), indicating impaired efferocytosis in *ApoE*$^{-/-}$ mice induced by Hcy. Next, we treated macrophages with Hcy and incubated them with green fluorescent-labeled ACs, in which apoptosis was induced by ultraviolet (UV) irradiation (Figure 1D). As expected, macrophage efferocytosis was impaired under Hcy treatment with a reduced capacity for clearing fluorescent ACs (Figure 1E). The decreased phagocytotic activity of macrophages was also verified by calcein-stained ACs (Figure 1F). Previous studies have shown that defective efferocytosis underlies a growing list of chronic inflammatory diseases and further exacerbates the progression of atherosclerosis. Therefore, we examined the effect of Hcy on macrophage inflammation, and increased expression of Il-6, Tnf-α and Ccl2 and decreased Arg1 and Il-10 expression were observed in macrophages treated with Hcy (Figure 1G). Collectively, these results demonstrate that Hcy suppressed macrophage efferocytosis in atherosclerosis.

lncRNA expression profiles are altered in Hcy-treated macrophages

To characterize lncRNA expression profiles in atherosclerosis induced by Hcy in *ApoE*$^{-/-}$ mice, we reanalyzed the lncRNA microarray data using an ensemble database (GRCh38_realease95) in 3 pairs of macrophages treated with/without Hcy. When we set the filter criteria as a fold-change ≥ 1.5 and a P value < 0.05, we found 80 differentially expressed lncRNAs, of which 42 were upregulated and 38 were downregulated in macrophages treated with Hcy (Figure 2A). Functional enrichment analysis (KOG, GO and KEGG pathway) of the target genes of the differentially expressed lncRNAs showed that there was a series of changes in the biological functions of macrophages by Hcy stimulation. As shown in Figure 2B, the target genes of these differentially expressed lncRNAs were categorized into 25 KOG clusters, and the five largest clusters were general function prediction only, signal transduction mechanisms, posttranslational modification, protein turnover, chaperones, translation, function unknown and transcription. For biological processes, the majority of lncRNA target genes were mainly involved in male gonad development, telomeric heterochromatin assembly and negative regulation of chromosome condensation. In the cell component class, in addition to the voltage-gated calcium channel complex, the endoplasmic reticulum membrane and bar body were both involved. For molecular functions, enriched GO terms included DNA binding, protein heterodimerization activity and ATP binding (Figure 2C). This indicated that the differentially expressed lncRNAs were involved in the metabolism of certain biomacromolecules. KEGG pathway analysis revealed that the differentially expressed lncRNAs were mainly involved in the metabolism of apoptosis and inflammation, including the p53 signaling pathway, PI3K-Akt signaling pathway, adipocytokine signaling pathway, FoxO signaling pathway, chemokine signaling pathway, and AGE-RAGE signaling pathway in diabetic complications. In particular, the target genes of differentially expressed lncRNAs were significantly enriched in apoptosis. More importantly, endocytosis contained a large number of genes in this pathway (Figure 2D). This finding implies that the differentially expressed lncRNAs are involved in the macrophage efferocytosis response to Hcy.

MAERL is upregulated in macrophage efferocytosis induced by Hcy

Furthermore, we analyzed the differentially expressed lncRNAs associated with efferocytosis. This analysis showed 7 differentially expressed lncRNA candidates in macrophages and then validated the sequencing results using qRT-PCR in atherosclerotic lesions of HMD-fed *ApoE*$^{-/-}$ mice. As a result, MSTRG.2814.24 was significantly upregulated (Figure 3A). Thus, we focused on MSTRG.2814.24 for further study, which was termed MAERL. Considering that the functions of lncRNAs depend on their characteristics, we first characterized MAERL by 5′ and 3′ RACE experiments in macrophages. The alignment results indicated that the full length of MAERL is 424 bases (Figure 3B and Supplementary Figure S1A). We then subjected the 424 bp MAERL sequence to a battery of bioinformatic analyses. Emerging evidence has revealed that the open reading frames (ORFs) inside lncRNAs can also encode micro peptides. Thus, we assessed MAERL for the presence of ORFs. However, there is no ORF longer than 200 bp in the sequence. Predicted peptide sequences were used to query the UniProtKB and Swiss-Prot databases, but no similarities to known proteins were found (Supplementary Figure S1B). The advanced structure of MAERL was predicted by RNAfold WebServer. We typed the RNA sequence and chose the options of fold algorithms, and the minimum free energy (MFE) structure and the centroid secondary structure were obtained (Supplementary Figure S1C). The computational algorithm of CPAT and CPC2 predict that MAERL has very low coding potential, similar to the well-known lncRNAs HOTAIR and TUG1 and much lower than protein coding ACTA1 and GAPDH (Figure 3C). Moreover, based on the UCSC Genome Browser, MAERL is located on chromosome 1 (p34.2) and is highly conserved among higher mammals (Figure 3D). Given that the subcellular localization of lncRNAs plays a vital role in predicting their molecular function, we evaluated the subcellular localization of MAERL. Cytoplasmic and nuclear RNA extraction experiments followed by RT-qPCR analysis showed that approximately 80% of the MAERL transcripts were in the nucleus (Figure 3E). FISH further demonstrated dual expression of MAERL in the cytoplasm and nucleus, with predominant enrichment in the cytoplasm (Figure 3F). Taken together, these results prompted us to study the function of MAERL in macrophage efferocytosis induced by Hcy.

MAERL silencing promotes macrophage efferocytosis

To demonstrate the functional role of MAERL in macrophage efferocytosis, MAERL LNA GapmeRs were constructed and transfected into macrophages treated with Hcy. Among these LNA GapmeRs, LNA-MAERL-1 was selected for subsequent experiments because it exhibited the strongest knockdown efficiency (Figure 4A). We then assessed continual efferocytosis by evaluating the ability of these macrophages to ingest ACs. LNA MAERL obviously enhanced the efferocytosis of macrophages for the calcein-stained ACs (Figure 4B). Double immunofluorescence staining revealed an approximately 30% increase in macrophages that ingested red ACs in the *MAERL* silencing group (Figure 4C). Moreover, *MAERL* silencing significantly reduced the inflammatory response of macrophages (Figure 4D). Taken together, these data demonstrate that LNA-MAERL promotes macrophage efferocytosis and inhibits inflammation in atherosclerosis.

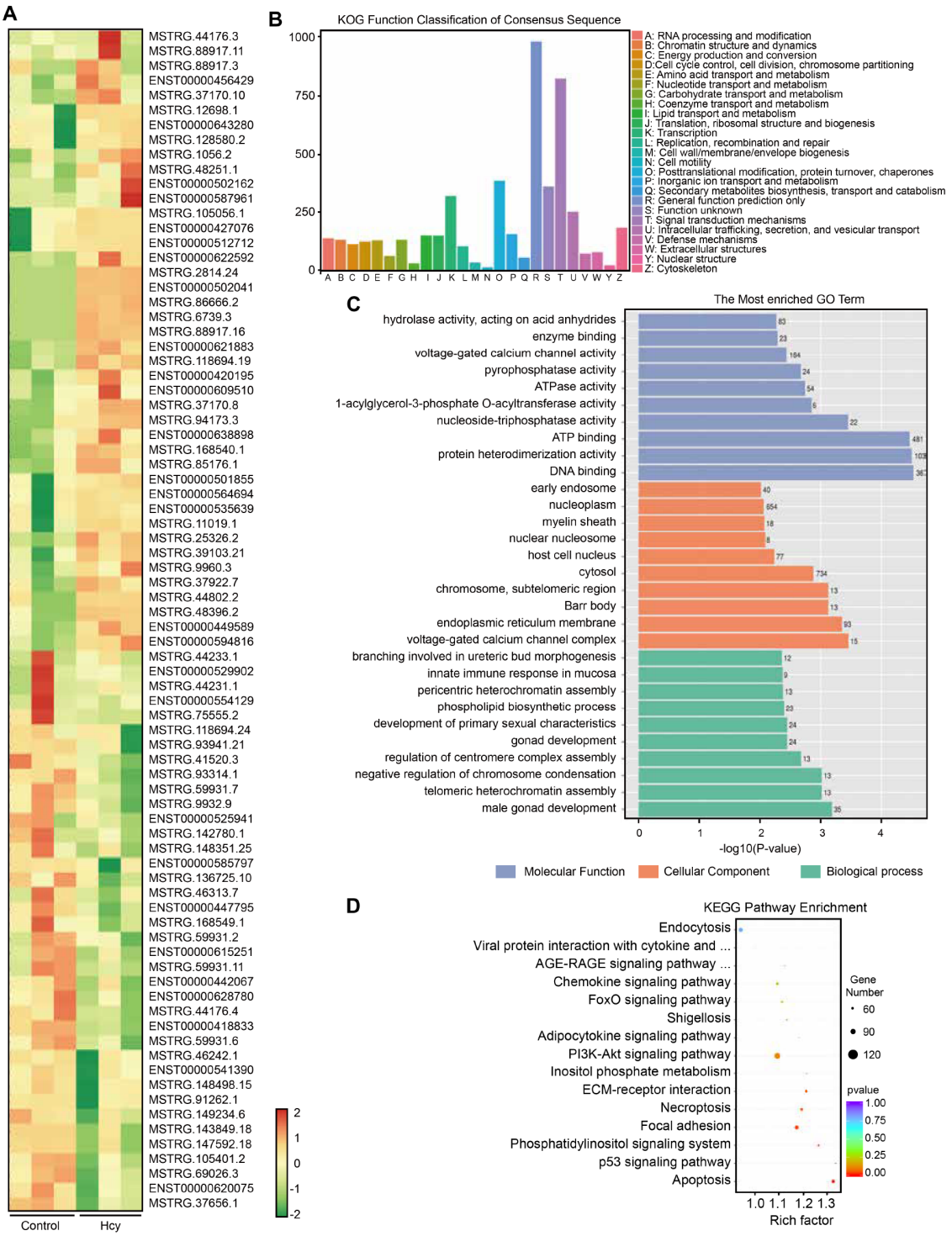

Figure 2. The differently expressed lncRNAs were involved in macrophages efferocytosis (A) Cluster heatmap of all differentially expressed lncRNAs in macrophages treated with/without Hcy. The red and green strips represented high and low expression, respectively. (B) KOG classification of differentially expressed lncRNAs. Eukaryotic Ortholog Groups (KOG) were divided into 25 groups, and the genes with successful KOG annotations were classified according to the KOG group. The horizontal axis is the names of the 25 groups of KOG, and the vertical axis is the proportion of the number of genes annotated to the group to the total number of genes annotated. (C) A histogram of GO enrichment analysis of differentially expressed lncRNAs. GO terms include biological processes, molecular functions, and cellular components. Vertical axis, the GO annotation; horizontal axis, –log10(P-value). (D) Scatter plot of KEGG enrichment analysis of differentially expressed lncRNAs. Horizontal axis, Rich factor. Rich factor indicates the ratio of the number of differential KEGG genes to the total number of KEGG genes. The larger the Rich factor, the greater the KEGG enrichment. Vertical axis, pathway term (the KEGG metabolic pathway). In the scatter plot, the dot size represents the number of genes with a significant difference.

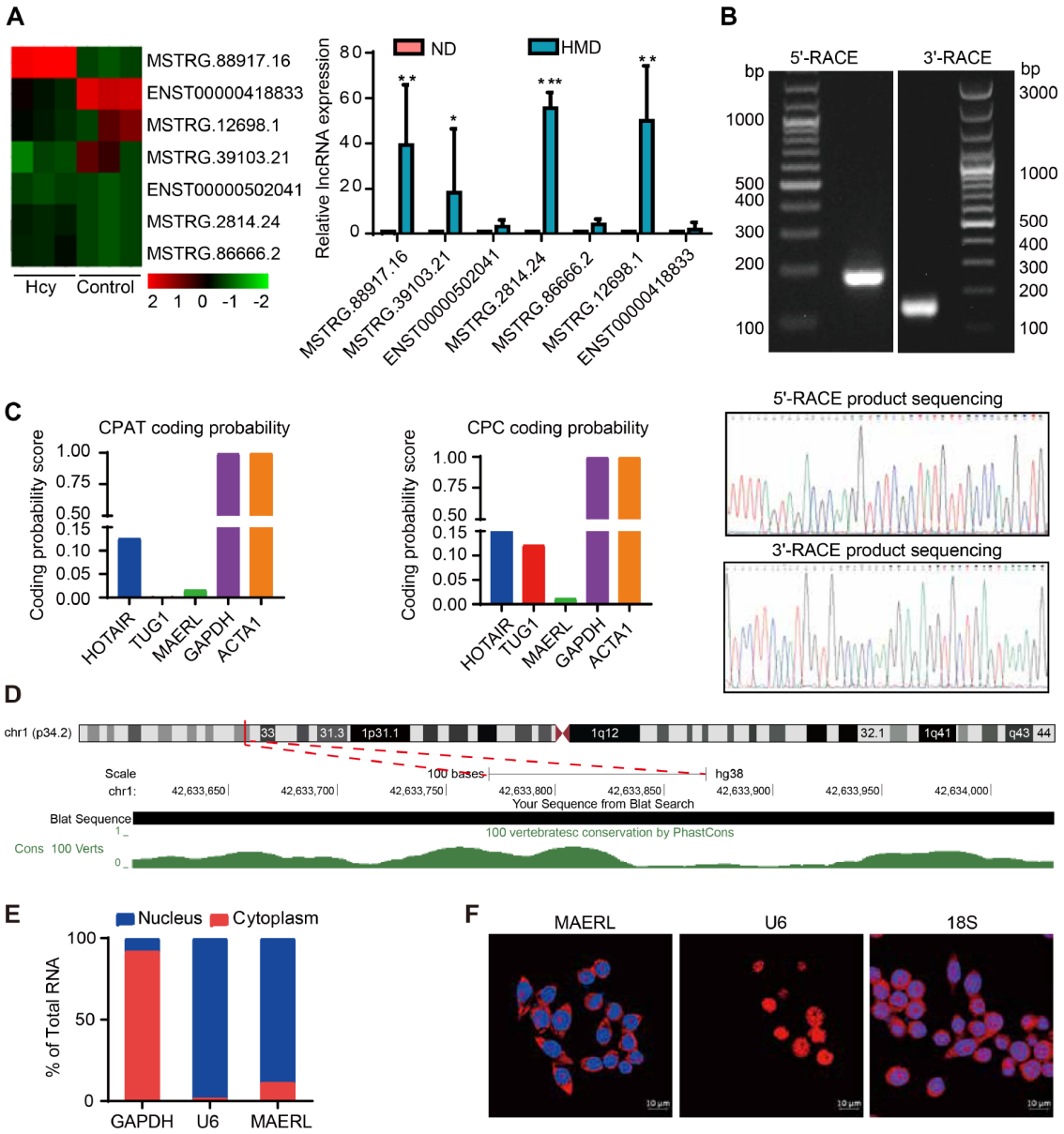

Figure 3. Detection and characterization of lncRNA MAERL (A) The cluster heatmaps showed the 7 differentially expressed lncRNAs which were associated with efferocytosis in macrophages with or without Hcy. The red and green strips indicate up-regulated and down-regulated lncRNAs, respectively. The expression of 8 dysregulated lncRNAs in atherosclerotic lesions of HMD-fed *ApoE*$^{-/-}$ mice measured by qRT-PCR. (B) 5′ and 3′ rapid amplification of cDNA end (RACE) assays in macrophages to detect the whole sequence of MAERL. (C) Protein-coding predictions for MAERL and comparator RNAs. Coding Potential Assessment Tool (CPAT) and Coding Potential Calculator 2 (CPC2) for MAERL, HOTAIR, TUG1, ACTA1 and GAPDH. HOTAIR and TUG1 served as noncoding RNA controls, while ACTA1 and GAPDH served as coding RNA controls. Using this algorithm, coding probability less than 1 are considered to identify non-coding RNAs. (D) The location of MAERL on human chromosome and the conservation between different higher mammals. (E) Subcellular location of MAERL by cytoplasmic and nuclear RNA separated extraction experiments followed by RT-qPCR analysis in macrophages. U6 and GAPDH were used as internal controls. (F) Subcellular localization of MAERL by FISH in macrophages. Special FISH probes against MAERL, U6, and 18S were modified by Cy3 (red); 18S is a cytoplasmic marker, and U6 is a nuclear marker. The nucleus was stained by DAPI (blue). Scale bar = 10 μm.*$P < 0.05$, **$P < 0.01$, ***$P < 0.001$.

MAERL interacts with and regulates TGM2 in Hcy-treated macrophages

Growing evidence has pointed to the notion that many lncRNAs can function to regulate the expression of some target genes through direct interactions with proteins [13,14]. To explore the potential binding proteins for MAERL in macrophages, we performed RNA pulldown using *in vitro*-transcribed MAERL RNA with a biotin-labeled 3′ end in macrophages followed by silver staining (Figure 5A) and analyzed the protein products by mass spectrometry. With the cutoff criteria of unique peptides ≥ 1 and –10lgP ≥ 13, we identified 114 unique proteins that were pulled down by probes specific for MAERL but not the negative control probe. In addition, the catRAPID database was used to predict potential proteins that may interact with MAERL, and 19 proteins were identified by mass

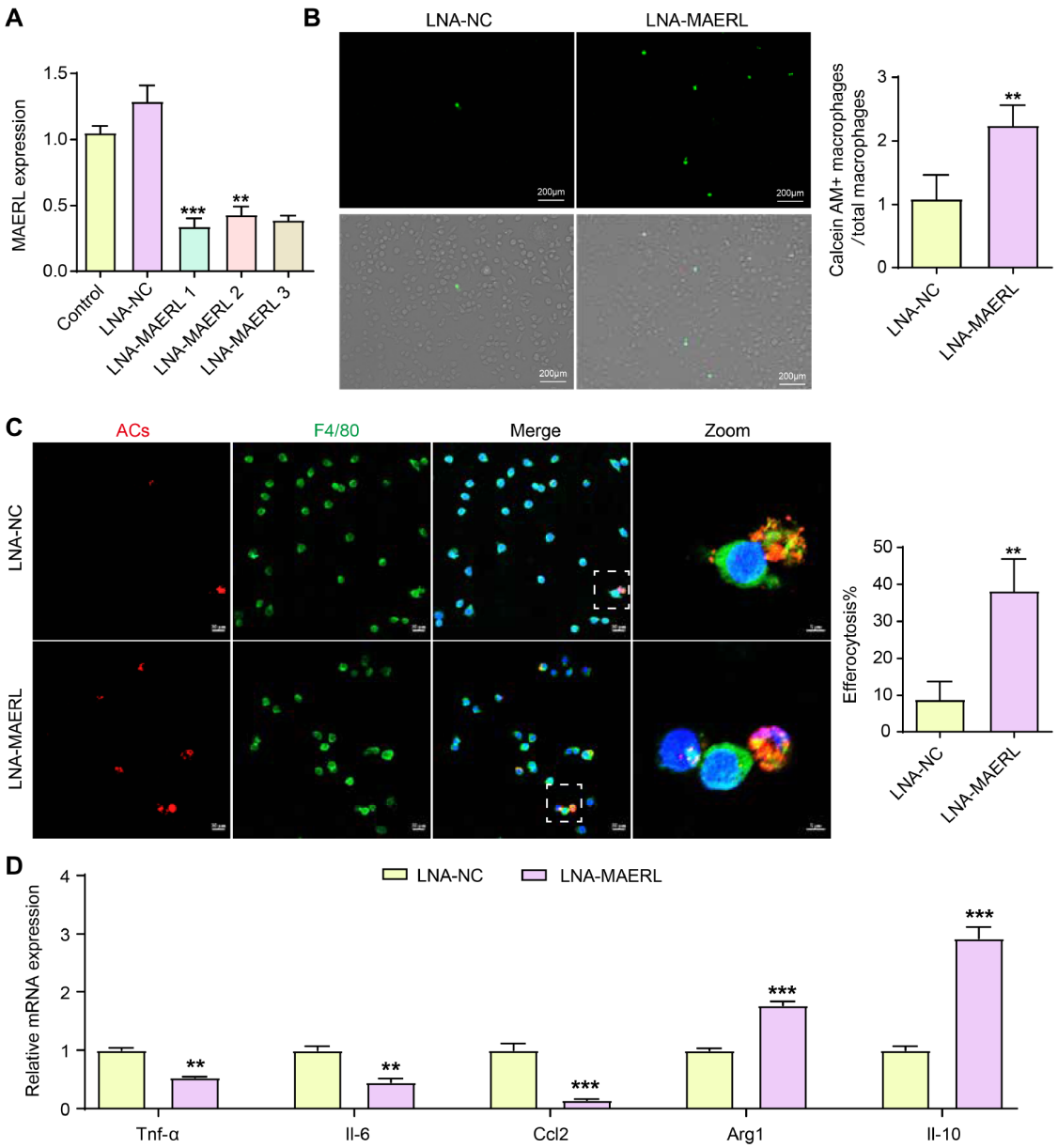

Figure 4. *MAERL* silencing restores Hcy-inhibited macrophage efferocytosis (A) Efficacy of *MAERL* knockdown with LNA GapmeRs in macrophages. (B) The efferocytosis assay of macrophages transfected with LNA-MAERL. Efferocytosis was quantified as the ratio of calcein-positive to calcein-negative macrophages. Scale bar = 200 μm. (C) *MAERL*-silenced macrophages that had or had not engulfed ACs were visualized by microscopy, and macrophages (green) were incubated with CFSE-labeled ACs (red). Scale bar = 20 μm. Zoom, scale bar = 5 μm. (D) qRT-PCR was performed to detect the mRNA levels of Il-6, Tnf-α, Ccl2, Il-10 and Arg1 in macrophages transfected with LNA-MAERL. $^{**}P < 0.01$, $^{***}P < 0.001$.

spectrometry (Supplementary Table S1). Among these proteins, four proteins (EF1A2, TGM2, ACTN4, and CRYAB) have been confirmed to be associated with efferocytosis (Figure 5B). For further investigation, EF1A2 and TGM2, which met the criterion of ≥ 3 unique peptides, were selected (Figure 5C,D). RNA pull-down assays showed that EF1A2 and TGM2 specifically bound to MAERL (Figure 5E). An RIP assay was further utilized to validate the specific interaction between MAERL and EF1A2 and TGM2 (Figure 5F). Next, we examined the expression of EF1A2 and TGM2 following *MAERL* knockdown in macrophages. The results showed that MAERL depletion significantly promoted TGM2 protein levels, while EF1A2 expression remained unchanged (Figure 5G). Notably, *MAERL* knockdown did not affect TGM2 mRNA levels (Figure 5H). In addition, TGM2 expression was decreased in macrophages treated with Hcy (Figure 5I). These findings suggest that MAERL interacts with and posttranscriptionally regulates TGM2 in Hcy-treated macrophages, implying a role for TGM2 in MAERL-mediated efferocytosis.

MAERL impairs macrophage efferocytosis through TGM2

Since MAERL shares TGM2 binding, we wondered whether TGM2 is involved in the MAERL-induced inhibition of macrophage efferocytosis. The rescue experiments were carried out by cotransfection

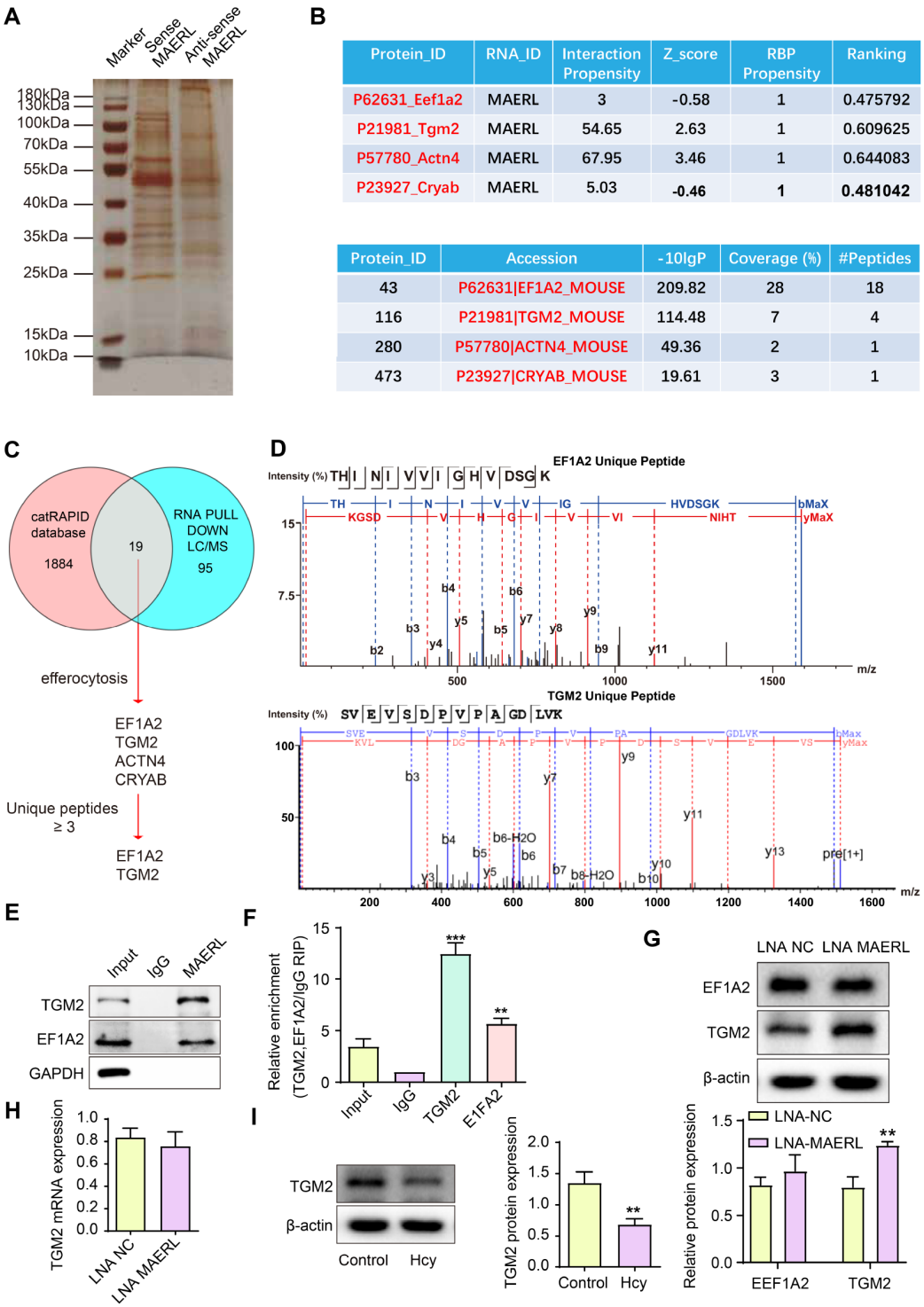

Protein_ID	RNA_ID	Interaction Propensity	Z_score	RBP Propensity	Ranking
P62631_Eef1a2	MAERL	3	-0.58	1	0.475792
P21981_Tgm2	MAERL	54.65	2.63	1	0.609625
P57780_Actn4	MAERL	67.95	3.46	1	0.644083
P23927_Cryab	MAERL	5.03	-0.46	1	0.481042

Protein_ID	Accession	-10lgP	Coverage (%)	#Peptides
43	P62631|EF1A2_MOUSE	209.82	28	18
116	P21981|TGM2_MOUSE	114.48	7	4
280	P57780|ACTN4_MOUSE	49.36	2	1
473	P23927|CRYAB_MOUSE	19.61	3	1

Figure 5. MAERL interacts with and inhibits TGM2 expression in macrophages treated with Hcy (A) RNA pull-down assay by MAERL and its antisense RNA followed by silver staining of protein extract from macrophages. A band indicated by an arrow was excised for mass spectrometry analysis. (B) The four proteins (EF1A2, TGM2, ACTN4, and CRYAB) associated with efferocytosis were found to interact with MAERL, as determined by RNA pull-down assay and predictive analysis via the catRAPID database. (C) Flowchart for the screening and identification of target proteins. (D) Identification of MAERL-interacting peptides of EF1A2 and TGM2 identified by mass spectrometry. (E) RNA pull-down assay followed by western blot analysis of the specific association of TGM2 and EF1A2 with MAERL. (F) RIP experiments were performed using antibodies against EF1A2 and TGM2 on macrophage extracts followed by qRT-PCR. IgG served as the negative control. (G) The expression of EF1A2 and TGM2 was detected by western blot analysis in macrophages transfected with MAERL LNA GapmeRs. (H) The mRNA expression of TGM2 in macrophages transfected with MAERL LNA GapmeRs was measured by qRT-PCR. (I) The expression of TGM2 in macrophages treated with Hcy was detected by western blot analysis. $^{**}P < 0.01$, $^{***}P < 0.001$.

with LNA-MAERL and si-TGM2. The efferocytosis assay revealed that *MAERL* silencing significantly promoted the phagocytotic activity of macrophages, as verified by calcein-stained ACs (Figure 6A). Additionally, we also observed decreased macrophage capacity for clearing fluorescent ACs in macrophages cotransfected with LNA-MAERL and si-TGM2 (Figure 6B). These results indicated that MAERL regulates macrophage efferocytosis in atherosclerosis by regulating TGM2 expression.

Discussion

Defective efferocytosis is a hallmark of advanced atherosclerotic plaques and plays a critical role in the progression of atherosclerosis across its various stages [15]. This cellular process is primarily regulated by specialized signaling pathways and membrane

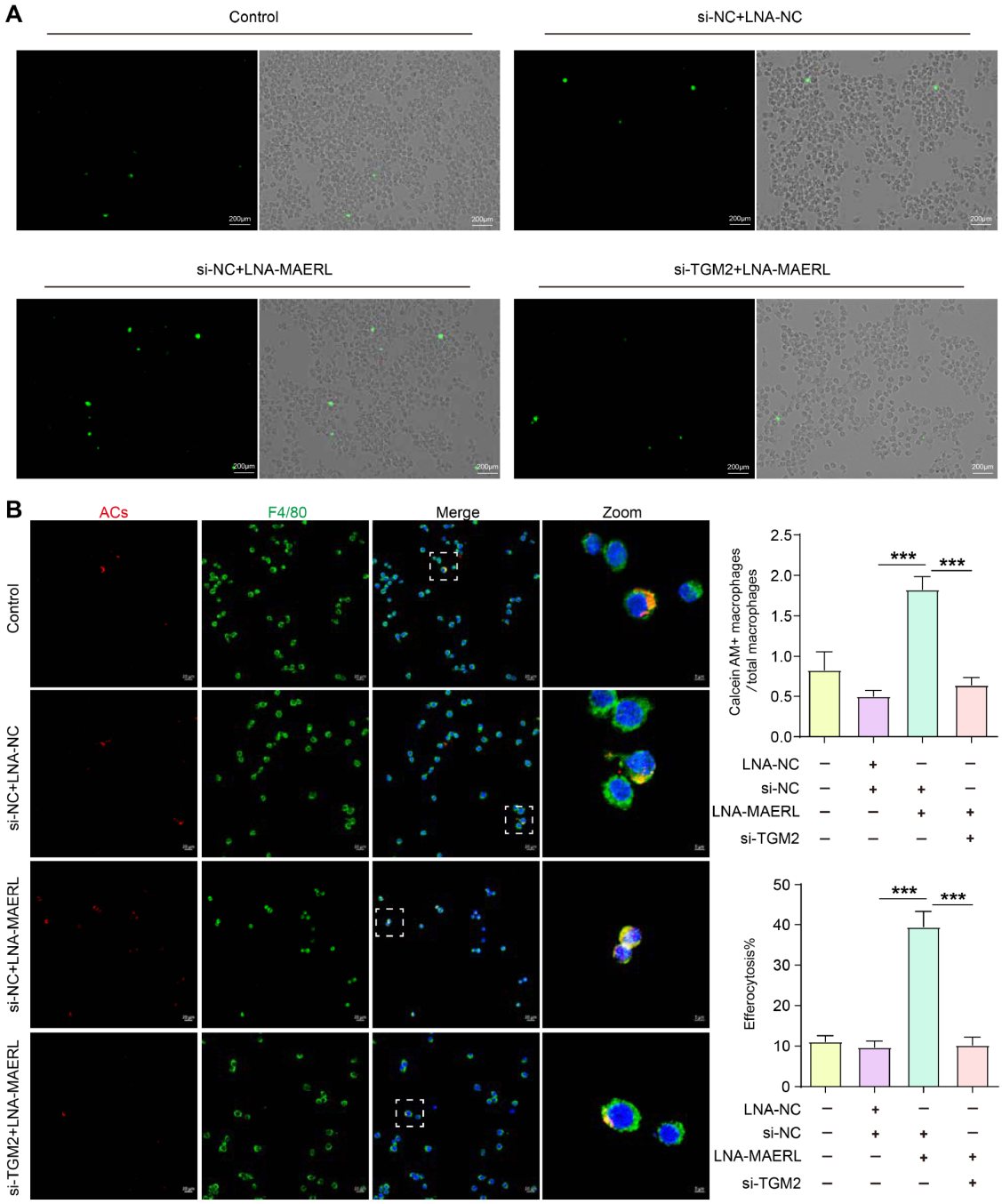

Figure 6. MAERL regulates macrophage efferocytosis in atherosclerosis by regulating TGM2 expression (A) The efferocytosis assay of macrophages co-transfected with LNA-MAERL and si-TGM2. Efferocytosis was quantified as the percentage of calcein-positive to calcein-negative macrophages. Scale bar = 200 μm. (B) Macrophages co-transfected with LNA-MAERL and si-TGM2 that had or had not engulfed ACs were visualized by microscopy, and macrophages (green) were incubated with CFSE-labeled ACs (red). Scale bar = 20 μm. Zoom, scale bar = 5 μm. ***$P < 0.001$.

receptors, which coordinate the recognition, engulfment, and degradation of apoptotic cells within plaques [16]. Multiple systemic and environmental factors have been shown to impair macrophage efferocytosis in atherosclerosis, with key examples including metabolic factors, environmental exposures, and chronic inflammatory or nutritional deficiency states. These diverse factors converge on common pathological mechanisms that alter macrophage phenotype, disrupt core efferocytosis pathways, induce metabolic reprogramming, or disturb inflammatory homeostasis, thereby directly compromising the efficiency of apoptotic cell clearance [17,18]. For instance, in mouse models, limiting PKM2 activity in myeloid cells under a high-fat western diet enhances apoptotic cell clearance and attenuates plaque formation [19]. Similarly, disturbed blood flow—a key mechanical feature of atherosclerosis—impairs MerTK-mediated efferocytosis in vascular endothelial cells, further contributing to local apoptotic cell accumulation and plaque vulnerability [20]. However, the systematic roles and mechanisms of efferocytosis in integrating these cues within human atherosclerosis remain to be fully elucidated.

Our previous studies have confirmed that a high-methionine diet can induce atherosclerosis, with mechanistic investigations revealing the involvement of autophagy [11], inflammation [21], and ferroptosis [22] in this process. However, whether it alters macrophage efferocytosis remains unclear. In the present study, we demonstrated that efferocytosis was significantly impaired in macrophages within atherosclerotic plaques of HMD-fed *ApoE*$^{-/-}$ mice as well as in macrophages treated with Hcy. Consistently, our results further revealed that the expression levels of proinflammatory cytokines (IL-1β, IL-6, and TNF-α) were markedly upregulated, while the expression of anti-inflammatory cytokines (IL-10 and Arg1) was significantly suppressed in macrophages from HMD-fed *ApoE*$^{-/-}$ mice and Hcy-treated macrophages. It is well established in atherosclerosis research that impaired efferocytosis leads to the accumulation of uncleared ACs in atherosclerotic plaques. The persistent accumulation of ACs subsequently triggers secondary necrosis, which is accompanied by the release of various damage-associated molecular patterns (DAMPs). These released DAMPs can serve as key danger signals to activate intracellular inflammasome complexes, thereby initiating and perpetuating local inflammatory responses within the plaque [4,5]. Our findings are consistent with this well-accepted pathogenic paradigm, reinforcing the important role of efferocytosis dysfunction in the inflammatory pathogenesis of atherosclerosis under Hcy-related conditions.

lncRNAs function as promotive or inhibitory regulators and have been reported to play central roles in plaque formation, necrotic core expansion, and clinical outcomes of cardiovascular diseases [23,24]. For example, lncARF has been shown to be essential for HHcy-impaired autophagy by targeting RRAGD signaling [11]. PSMB8-AS1, another lncRNA, is closely associated with enhanced vascular inflammation and plaque stability in mouse models [25]. However, the regulatory functions of lncRNAs in macrophage efferocytosis during atherosclerosis remain largely unexplored. One notable exception is the report by Yin *et al.* [26], which identified lncRNA SCARNA8 as a promoter of atherosclerotic plaque instability through its inhibition of macrophage efferocytosis. In the present study, through lncRNA sequencing of Hcy-treated macrophages, we identified MAERL as a novel lncRNA responsive to Hcy stimulation. Notably, MAERL expression was significantly upregulated in macrophages exposed to Hcy. To elucidate its functional and molecular role, we characterized the full-length transcript of MAERL using RACE and the encoding ability using the Coding Potential Assessment Tool (CPAT), Contrastive Predictive Coding (CPC) and other bioinformatics analyses. Furthermore, we demonstrated that MAERL is functionally linked to macrophage efferocytosis and that knockdown of *MAERL* markedly enhanced efferocytic activity. Collectively, these results suggest that MAERL may contribute to Hcy-induced atherosclerosis by negatively regulating efferocytosis in macrophages.

The function of lncRNAs is closely linked to their subcellular localization. For instance, the cytoplasm-enriched lncRNA Malat1 regulates the transition of Sca1^{+} progenitor cells to vascular smooth muscle cells during vascular remodeling [27]. Similarly, H19, another lncRNA primarily expressed in the cytoplasm, has been reported to be epigenetically upregulated in SAHH deficiency, promoting Runx2-dependent atherosclerotic calcification [28]. In this study, we found that MAERL is distributed in both the nucleus and cytoplasm of macrophages, with predominant localization in the cytoplasm. This suggests that MAERL may primarily participate in atherosclerosis progression through interactions with cytoplasmic proteins and regulation of their functions. To identify proteins that interact with MAERL, we performed RNA pulldown combined with mass spectrometry (MS) analysis and utilized the catRAPID omics platform. The results were further validated by RIP. Based on MS data and bioinformatic predictions, we identified and confirmed that TGM2 interacts with MAERL and is functionally regulated by it. Notably, a recent study reported that TGM2 serves both as a marker of efferocytosis and a target for efferocytosis inhibition in hypoxia-induced glioblastoma [29]. However, whether TGM2 is involved in MAERL-regulated macrophage efferocytosis remains unclear. In our experiments, silencing *TGM2* attenuated the enhanced efferocytosis induced by *MAERL* knockdown, indicating that TGM2 contributes to the regulatory effect of MAERL on macrophage efferocytosis. Notably, *MAERL* knockdown did not alter TGM2 mRNA levels, suggesting that this regulation occurs at the posttranscriptional level. Our study provides potential therapeutic targets for atherosclerosis by revealing a novel signaling axis of TGM2 that is regulated by MAERL.

However, it is important to acknowledge the limitations of this study. Our mechanistic findings are primarily derived from *in vitro* models and murine systems; thus, further validation in human atherosclerotic plaques and primary human macrophages is essential to confirm translational relevance. Additionally, while MAERL/TGM2 represents a promising target, the practical challenges of achieving tissue-specific delivery and pharmacological modulation of a nuclear-retained lncRNA *in vivo* must be thoroughly addressed in future translational studies.

In summary, we provide a lncRNA landscape of Hcy-treated macrophages and identify a novel lncRNA, MAERL, that is able to inhibit macrophage efferocytosis. Mechanistically, we demonstrate that MAERL interacts with TGM2 to reduce TGM2 expression, finally contributing to impaired macrophage efferocytosis, revealing a novel MAERL/TGM2 signaling axis and identifying it as a potential therapeutic target for atherosclerosis.

Supplementary Data

Supplementary data are available at *Acta Biochimica et Biophysica Sinica* online.

Data Availability

In compliance with the journal's policy, we state the restriction that the raw data cannot be publicly shared at present due to their involvement in other unpublished manuscripts (privacy/contractual constraints related to ongoing work). To provide a managed-access pathway, data can be accessed upon reasonable request from the corresponding authors. Furthermore, where possible, we will deposit metadata and/or deidentified or aggregated data into a suitable database (to be specified) upon the completion of the related unpublished work.

Acknowledgement

The authors acknowledge NHC Key Laboratory of Metabolic Cardiovascular Diseases Research and Ningxia Key Laboratory of Vascular Injury and Repair Research for assistance with instrumentation.

Author Contributions

KX developed the initial concept, designed and performed the experiments, and analyzed the data. YJW and QQW developed the initial concept, designed and performed the experiments, and drafted the manuscript. ZHZ, SJL, JQY and XYZ were responsible for immunohistochemistry, cell culture and collection of data. GZL and JMS contributed reagents, materials and analysis tools. GZL and QQW supported finance and revised the manuscript. FM developed the initial concept, designed the experiments, and drafted the manuscript. SCM and GDZ developed the initial concept and revised the manuscript.

Funding

This work was supported by the grants from the National Major Science and Technology Program (No. 2024ZD0531200), the National Natural Science Foundation of China (Nos. 82571009, 82360628, 82160687), the Key Research and Development Projects in Ningxia Province (Nos. 2023BEG02074, 2022BEG02054, and 2023BSB03042), the Open Competition Mechanism to Select the Best Candidates for Key Research Projects of Ningxia Medical University (No. XJKF240311), and the Key Research Projects of Ningxia Medical University (No. XZ2022005).

Conflict of Interest

The authors declare that they have no conflict of Interest.

References

1. Tian W, Ju J, Guan B, Wang T, Zhang J, Song L, Xu H. Role of hyperhomocysteinemia in atherosclerosis: from bench to bedside. *Ann Med* 2025, 57: 2457527
2. Yuan D, Chu J, Lin H, Zhu G, Qian J, Yu Y, Yao T, *et al.* Mechanism of homocysteine-mediated endothelial injury and its consequences for atherosclerosis. *Front Cardiovasc Med* 2022, 9: 1109445
3. Mengstu MK, Girmay G, Altaye KD, Habtu W, Tolcha Y, Getnet E, Lemma M, *et al.* Comparison of inflammatory cells, C-reactive protein, and lipid profile in atherosclerotic cardiovascular disease patients and healthy controls in northwest ethiopia. *Sci Rep* 2025, 15: 37448
4. Gerlach BD, Ampomah PB, Yurdagul Jr. A, Liu C, Lauring MC, Wang X, Kasikara C, *et al.* Efferocytosis induces macrophage proliferation to help resolve tissue injury. *Cell Metab* 2021, 33: 2445–2463.e8
5. Bao Q, Zhang B, Zhou L, Yang Q, Mu X, Liu X, Zhang S, *et al.* CNP ameliorates macrophage inflammatory response and atherosclerosis. *Circ Res* 2024, 134: e72
6. Watmuff H, Crawford A, Eusse B, Jones AN. Structure-function-guided drug development efforts to target lncRNAs. *Trends Pharmacol Sci* 2025, 46: 703–721
7. Han JDJ. LncRNAs: the missing link to senescence nuclear architecture. *Trends Biochem Sci* 2023, 48: 618–628
8. Nossent AY, Binder CJ. Noncoding RNAs in atherosclerosis. *Atherosclerosis* 2023, 374: 21–23
9. Ni H, Ge Y, Zhuge Y, Liu X, Chen H, Liu J, Li W, *et al.* LncRNA MIR181A1HG deficiency attenuates vascular inflammation and atherosclerosis. *Circ Res* 2025, 136: 862–883
10. Zhang R, Bu F, Wang Y, Huang M, Lin X, Wu C, Chen J, *et al.* LncRNA RP4-639F20.1 interacts with THRAP3 to attenuate atherosclerosis by regulating c-FOS in vascular smooth muscle cells proliferation and migration. *Atherosclerosis* 2023, 379: 117183
11. Ding N, Ma S, Chang Q, Xie L, Li G, Hao Y, Xiong J, *et al.* Novel long noncoding lncARF mediated hyperhomocysteinemia-induced atherosclerosis via autophagy inhibition in foam cells. *J Adv Res* 2025, 73: 311–328
12. Xu Y, Chen J, Liu Y, Zhang G, Miao G, Wu J, Lu K, *et al.* The macrophage-derived motor protein KIF13B enhances MERTK-mediated efferocytosis and prevents atherosclerosis in mice. *Eur Heart J* 2025: ehaf523
13. Zhao J, Sun J, Shuai SC, Zhao Q, Shuai J. Predicting potential interactions between lncRNAs and proteins via combined graph auto-encoder methods. *Brief Bioinform* 2023, 24: bbac527
14. Ma F, Liu H, Xia T, Zhang Z, Ma S, Hao Y, Shen J, *et al.* HSFAS mediates fibroblast proliferation, migration, trans-differentiation and apoptosis in hypertrophic scars via interacting with ADAMTS8. *Acta Biochim Biophys Sin* 2024, 56: 440–451
15. Lv JJ, Wang H, Zhang C, Zhang TJ, Wei HL, Liu ZK, Ma YH, *et al.* CD147 sparks atherosclerosis by driving M1 phenotype and impairing efferocytosis. *Circ Res* 2024, 134: 165–185
16. Wang Y, Liu XY, Wang Y, Zhao WX, Li FD, Guo PR, Fan Q, *et al.* NOX2 inhibition stabilizes vulnerable plaques by enhancing macrophage efferocytosis via MertK/PI3K/AKT pathway. *Redox Biol* 2023, 64: 102763
17. He Z, Luo Y, Duan Z, Su B, Zeng W, Guo Y, Li Y, *et al. IRF5* siRNA nanoimmunotherapy: restoring macrophage efferocytosis in atherosclerosis. *Circulation* 2025, 152: 1564–1581
18. Cao DY, Khan Z, Li X, Saito S, Bernstein EA, Victor AR, Ahmed F, *et al.* Macrophage angiotensin-converting enzyme reduces atherosclerosis by increasing peroxisome proliferator-activated receptor α and fundamentally changing lipid metabolism. *Cardiovasc Res* 2023, 119: 1825–1841
19. Doddapattar P, Dev R, Ghatge M, Patel RB, Jain M, Dhanesha N, Lentz SR, *et al.* Myeloid cell PKM2 deletion enhances efferocytosis and reduces atherosclerosis. *Circ Res* 2022, 130: 1289–1305
20. Wu J, Liu S, Banerjee O, Shi H, Xue B, Ding Z. Disturbed flow impairs MerTK-mediated efferocytosis in aortic endothelial cells during atherosclerosis. *Theranostics* 2024, 14: 2427–2441
21. Liu D, Yang A, Li Y, Li Z, You P, Zhang H, Quan S, *et al.* Targeted delivery of rosuvastatin enhances treatment of hyperhomocysteinemia-induced atherosclerosis using macrophage membrane-coated nanoparticles. *J Pharm Anal* 2024, 14: 100937
22. Yang A, Zhang H, Zhang H, Li N, Chen C, Yang X, Tian J, *et al.* Pitavastatin and resveratrol bio-nanocomplexes against hyperhomocysteinemia-induced atherosclerosis via blocking ferroptosis-related lipid deposition. *J Control Release* 2025, 381: 113598
23. Qu W, Zhou X, Jiang X, Xie X, Xu K, Gu X, Na R, *et al.* Long noncoding RNA Gpr137b-ps promotes advanced atherosclerosis via the regulation of autophagy in macrophages. *Arterioscler Thromb Vasc Biol* 2023, 43

24. Zhang W, Zhao J, Deng L, Ishimwe N, Pauli J, Wu W, Shan S, *et al.* *INKILN* is a novel long noncoding rna promoting vascular smooth muscle inflammation via scaffolding MKL1 and USP10. *Circulation* 2023, 148: 47–67
25. Li S, He RC, Wu SG, Song Y, Zhang KL, Tang ML, Bei YR, *et al.* LncRNA *PSMB8-AS1* instigates vascular inflammation to aggravate atherosclerosis. *Circ Res* 2024, 134: 60–80
26. Yin X, Chen X, Wang T, Yang J, Yu J, Yang J. LncRNA SCARNA8 promotes atherosclerotic plaque instability by inhibiting macrophage efferocytosis. *Epigenetics* 2025, 20: 2487317
27. Lyu L, Li Z, Wen Z, He Y, Wang X, Jiang L, Zhou X, *et al.* Fate mapping RNA-sequencing reveal Malat1 regulates Sca1+ progenitor cells to vascular smooth muscle cells transition in vascular remodeling. *Cell Mol Life Sci* 2023, 80: 118
28. Dai X, Liu S, Cheng L, Huang T, Guo H, Wang D, Xia M, *et al.* Epigenetic upregulation of H19 and AMPK inhibition concurrently contribute to S-adenosylhomocysteine hydrolase deficiency-promoted atherosclerotic calcification. *Circ Res* 2022, 130: 1565–1582
29. Lui M, Sevinc F, Elgafarawi M, Munoz DG, Keillor JW, Sinclair J, Catana D, *et al.* Transglutaminase 2 function in glioblastoma tumor efferocytosis. *Cell Death Dis* 2025, 16: 487